News Journal, International Society for Rock Mechanics (ISRM). Vol. 7, no. 2, June 2002. page 9 - 23

Laboratory Study of Geometrical and Hydro-Mechanical Characteristics of Discontinuities

By Marco V. Vicente Silvestre[1], Luis Ribeiro e Sousa[2] and Robert Hack[3]

Introduction

The presence and flow of water is very important for large hydraulic structures, e.g., hydroelectric schemes, pressure tunnels and shafts. These structures are affected by and effect the seepage of water through the surrounding rock mass. In general the rock mass can be characterized by a coupled mechanical-hydraulic-thermal-chemical behavior. For this research, relating to high-pressure tunnels of hydroelectric schemes, temperature differences are not significant and chemical alterations are practically not present. Hence, this paper focuses on the hydro-mechanical behavior only. To characterize the mechanical and hydraulic behavior of a rock mass it is necessary to consider the network of interconnected discontinuities. Generally, these are the most sensitive elements with respect to deformation under stress change and have a higher conductivity compared to the intact rock material. To understand the water flow through a network of discontinuities it is fundamental to analyze the mechanisms that determine the flow through a single discontinuity as function of stress. Geometrical properties of discontinuities, in particular roughness and aperture, have a significant influence on this behavior.

A laboratory study was initiated to provide geometrical and hydro-mechanical characteristics of single discontinuities that could be incorporated in a numerical model to simulate the small-scale flow through a single discontinuity as part of a network of discontinuities. This paper briefly describes the laboratory equipment utilized to obtain roughness and aperture characteristics of various discontinuities and the equipment utilized to obtain hydro-mechanical properties of these discontinuities. The obtained roughness data was analyzed using statistical parameters and roughness indexes by means of a finite element technique. An apparent aperture was determined by numerically matching the discontinuity surfaces and then the aperture data was analyzed with statistical parameters. The validity of the cubic law was studied and a power law was applied to fit the discontinuity transmissivity as function of stress.

1. Standard Testing and Engineering Company, Tulsa, OK, USA.
2. Laboratorio Nacional de Engenharia Civil (LNEC), Lisbon, Portugal
3. International Institute for Aerospace Survey and Earth Sciences (ITC), Delft, The Netherlands.

Sample Material

Rock samples with a natural discontinuity were selected from borehole cores that were taken from the rock mass in the area of the pressure tunnel of the Castelo do Bode dam site and the new underground powerhouse complex of the Miranda hydroelectric scheme in Portugal (Figure 1).

The rock material has a granular texture, with a well-defined foliation of micas, is slightly weathered and is classified as granitic gneiss. Also intact rock material cores from the Castelo do Bode site were selected to induce tension discontinuities by compressing the intact rock core with controlled piston velocity along the longitudinal core axis. All samples were cored with a 54 mm inside diameter diamond bit core barrel and cut to a length of approximately 112 mm. A total number of ten samples was obtained including seven natural and three induced tension discontinuities. Discontinuity type and origin of the sample material is summarized in Table 1.

Geometrical Characterization

Roughness Characterization

Surface Profiling

The profiling technique is a commonly used and relatively simple method to obtain topography data of discontinuity surfaces. The equipment utilized for this study obtained and stored fully-automatically three-dimensional surface topography data by means of a mechanical needle [1]. The device obtained surface data in an axial scanning approach by moving the needle along parallel lines, which were separated by a constant distance. A reading was stored only when the height difference between

Figure 1. Site Locations in Portugal

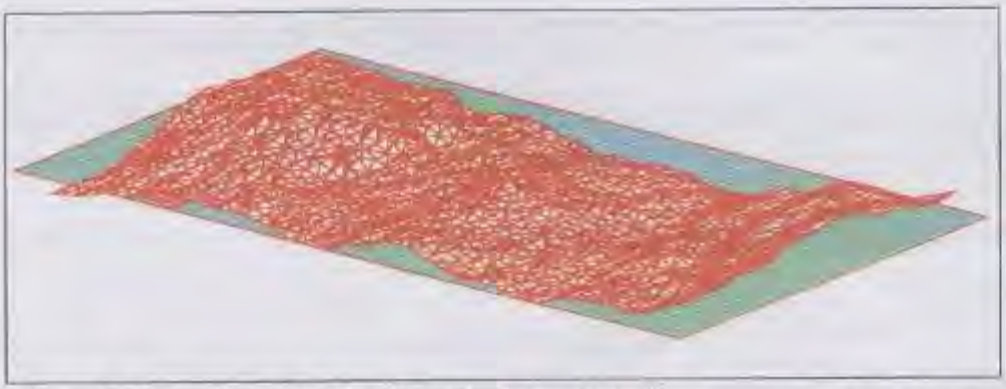

Figure 2. Triangular mesh of a discontinuity surface of sample CE

two successive points was less than a predefined value, otherwise the probe moved back to a position in between the two points and a new measurement was made. This procedure was repeated until the difference was less than the predefined value. The data points were, as a consequence of this procedure, irregularly spaced along a scanline. The selected probe had a radius of 1 mm, and the maximum scanning interval and maximum distance between the scanlines was set to 2 mm. The height measurement accuracy was generally in the order of microns. However, lower accuracies may have been obtained due to for example a concave shaped surface morphology. A local coordinate system, associated with the regression plane of all data points, was defined for both discontinuity halves. To allow a graphical representation of the surfaces, as well as to perform further computations, a triangular finite element mesh was generated (Figure 2). The computation of statistical parameters and roughness indexes was then performed using a finite element technique.

Asperity height distribution

The variance σ^2, coefficient of skewness a_3 and coefficient of kurtosis a_4 [2, 3, and 4] were calculated with a finite element technique using a numerical integration approach with Gaussian points [5]. With this approach the irregular sample density would not affect the parameter values. Within each defined triangle it was assumed that the height variation could be described with a linear function. The statistical parameters for each discontinuity surface are shown in Table 2.

Sample	Disc. Type	Original Location	Sample Depth (meters)
MA*	Natural	Miranda	20
MB	Natural	Miranda	20
MC	Natural	Miranda	20
MD	Natural	Miranda	20
ME	Natural	Miranda	20
CA*	Natural	Castelo do Bode	34
CB**	Natural	Castelo do Bode	65
CC	Induced	Castelo do Bode	34
CD	Induced	Castelo do Bode	61.5
CE**	Induced	Castelo do Bode	61.5

Table 1. Sample Type and Origin

The following becomes evident from these results: (1) the opposing discontinuity surfaces appear to be very similar; (2) generally, the planar natural discontinuities have low variance values ranging from 0.1 to 0.5 mm²; (3) for the stepped and undulating natural discontinuities (MA, CA, and CB) the variance increased significantly to values ranging from 1 to 10 mm²; (4) the planar induced tension discontinuities have clearly higher variance values in the order of 1.5 mm² compared with the planar natural discontinuities; and (5) the coefficient of skewness has both positive and negative values and the values of the coefficient of kurtosis are greater and less than 3. Therefore, no particular asperity height distribution could be distinguished.

Roughness Indexes

Roughness Indexes characterize the magnitude and texture of the surface morphology of discontinuities. A single index cannot fully describe the roughness. Hence, several indexes, each quantifying a different aspect of the morphology, should be selected. Magnitude indexes include the absolute roughness k, [6],the Central Line Average CLA, and Root Mean Square z_1. Texture indexes include the root mean square of the first derivative z_2, the root mean square of the second derivative z_3, and the portion of the surface with a positive slope minus the portion of the surface with a negative slope z_4.[7]. Another parameter associated with the surface geometry is R_A, the true area of the discontinuity wall to the base area projected on a reference plane. The surface morphology of side "A" was characterized with two-dimensional integral formulas of the indexes and a finite element technique. For indexes

Sample	Disc. Type	Surface	σ^2 (mm²)	a_3	a_4
MA	Natural	A	1.053	0.413	2.753
		B	1.073	0.338	2.728
MB	Natural	A	0.618	-0.133	2.194
		B	0.577	-0.067	2.175
MC	Natural	A	0.172	0.107	3.054
		B	0.166	0.374	3.556
MD	Natural	A	0.582	-0.171	2.725
		B	0.511	-0.106	2.553
ME	Natural	A	0.236	0.074	2.921
		B	0.278	-0.002	3.073
CA	Natural	A	4.866	0.931	3.648
		B	4.736	0.898	3.691
CB	Natural	A	10.030	-0.240	1.720
		B	10.158	-0.260	1.782
CC	Induced	A	1.461	0.166	2.404
		B	1.424	-0.048	2.247
CD	Induced	A	1.722	0.133	3.054
		B	1.742	0.069	3.029
CE	Induced	A	4.044	-0.352	2.662
		B	4.028	-0.297	2.641

Table 2. Asperity Height Distribution

Sample	k (mm)	CLA (mm)	z_1 (mm)	z_2 (-)	z_3 (mm^{-1})	z_4 (-)	R_A (-)
MA	5.548	0.834	1.027	0.166	0.148	0.073	1.020
MB	4.207	0.667	0.786	0.120	0.117	0.068	1.015
MC	3.139	0.340	0.414	0.096	0.094	0.012	1.009
MD	4.139	0.617	0.763	0.106	0.096	0.024	1.010
ME	2.787	0.377	0.486	0.097	0.093	0.056	1.007
CA	12.238	1.688	2.123	0.333	0.320	0.038	1.063
CB	12.116	2.820	3.172	0.278	0.172	0.059	1.048
CC	6.141	0.997	1.210	0.255	0.233	0.022	1.041
CD	7.450	1.042	1.333	0.296	0.261	-0.040	1.057
CE	10.797	1.648	2.011	0.329	0.286	0.064	1.068

Table 3. Roughness Indexes

Sample	E_a (mm)	E_h (mm)	σ^2 (mm^2)	a_3 (-)	a_4 (-)
MA	0.742	0.431	0.261	2.174	10.445
MB	0.269	0.170	0.039	1.935	7.962
MC	0.468	0.281	0.135	2.372	10.361
MD	0.431	0.284	0.068	1.221	5.247
ME	0.362	0.258	0.057	2.281	9.737
CA	0.575	0.469	0.059	0.741	4.091
CB	0.734	0.620	0.060	0.057	2.925
CC	1.706	1.079	0.633	0.129	2.737
CD	0.742	0.573	0.108	0.907	5.373
CE	0.521	0.454	0.033	1.071	9.313

Table 4. Aperture Distribution

z_2, z_3, and z_4, the defined direction corresponds with the longitudinal axis of the sample. The index values of each discontinuity are shown in Table 3.

Data analysis reveals a clear difference between the induced tension discontinuities and the natural discontinuities. It should be noted again that the index values of samples CA, CB, and CE reflect the undulating feature rather than the geometrical characteristics of the asperities. Generally, it can be said that the induced tension discontinuities have significant larger and sharper asperities and a more irregular texture.

Correlation of Roughness with JRC

The Joint Roughness Coefficient JRC is obtained with experimental pull tests [8] whereas the roughness indexes are calculated based on the surface morphology data only. The roughness indexes CLA, z_2, and R_A were selected to find a correlation with the JRC. Since both discontinuity surfaces affect the JRC, the average value of the indexes of the opposing discontinuity surfaces was used. The following linear correlations were found between the JRC and each roughness index:

JRC = 4.9138 CLA + 1.5333 (correlation coefficient 0.875)

JRC = 25.65 z_2 + 0.8652 (correlation coefficient 0.953)

JRC = 105.28 R_A + 102.77 (correlation coefficient 0.925)

Other correlations were reported by several authors [2, 3, 9, 10].

Aperture Characterization

Based on the obtained profiling data, the apparent aperture was numerically determined. The opposing digitized discontinuity surfaces were numerically matched and the aperture calculated as the difference between the opposing points with reference to the mean of the regression planes of the surfaces [1, 2, 3]. It should be noted that an apparent aperture was obtained that may differ from the actual aperture due to the following: (1) the opposing surfaces are numerically matched, which introduces assumptions with regard to what is considered the best fit; (2) the aperture is calculated with reference to a regression plane, thus the calculated apertures are not perpendicular to the local direction of the discontinuity; and (3) the aperture depends on the applied stress, which for this method is considered equal to zero.

Figure 3 presents a typical aperture distribution as obtained for samples MB and CE. Note the presence of narrow channels in a preferred direction for the natural discontinuity sample MB. This was not seen in the artificial tension discontinuities.

A statistical analysis was performed to characterize the aperture distribution. Table 4 presents the obtained values of the arithmetic mean E_a, harmon-

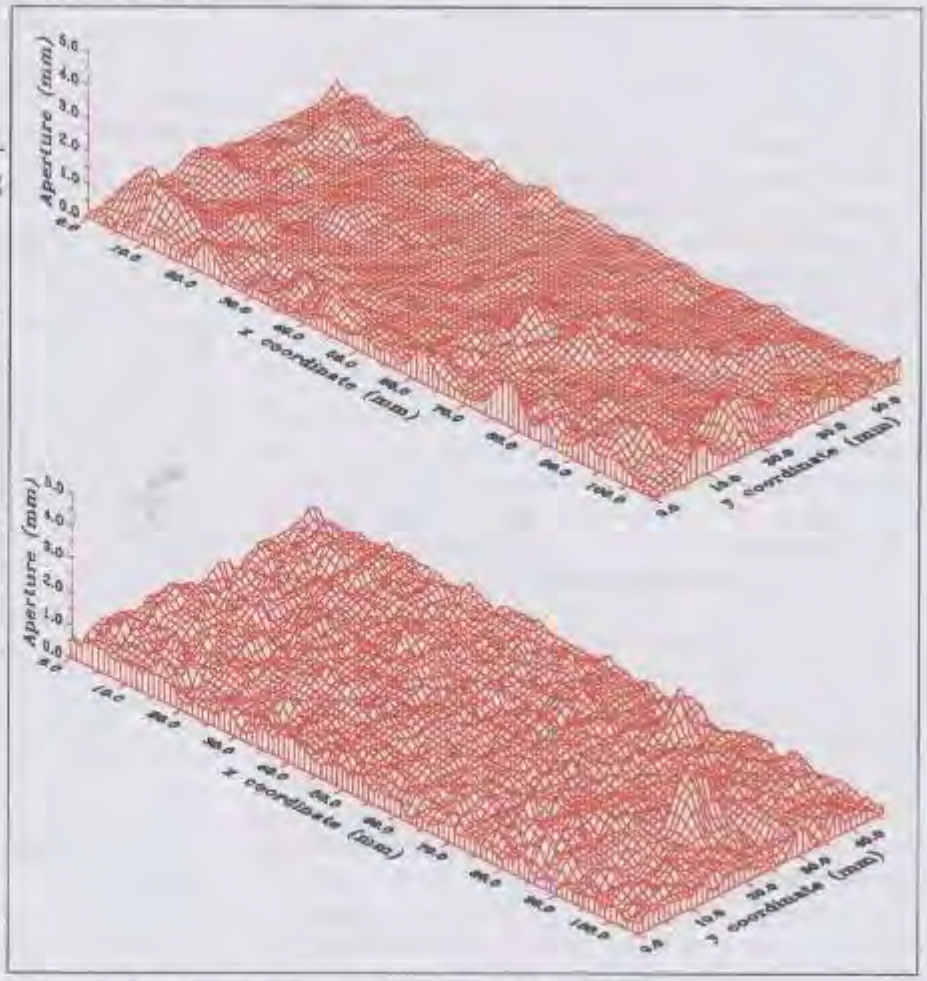

Figure 3. Aperture distribution of samples MB and CE

ic mean E_h, variance σ^2 and coefficients of skewness a_3 and kurtosis a_4.

The harmonic mean is considered more appropriate, since this mean diminishes the influence of accidentally high aperture values that might have been caused by the loss of material resulting from sample handling [2].

Analysis of the data reveals that all aperture distributions are right tailed with a high concentration around the mean aperture. These results are in agreement with other reported aperture distributions [11]. It should be noted that the high mean aperture values of sample CC are very likely caused by the loss of rock material during the process of inducing the tension discontinuity.

Hydro-Mechanical Characterization

Laboratory Testing Set-up

A cylindrical rock core, with a discontinuity along the longitudinal core axis, was placed in a triaxial cell. A confining pressure was applied to the rock core by pressurizing hydraulic oil around the sample. A stiff loading frame provided an axial load to the sample via an upper and a lower piston. In addition to the axial loading and confining pressure, the test set-up generated a water flow through the discontinuity from the bottom to the top. The flow rate at each loading cycle was measured at the top of the sample with three flow meters, each with a different capacity. For very low flow rates a weight balance was used which allowed the amount of water passed to be determined at certain time intervals. Two external linear variable differential transducers (LVDT) measured the axial displacements and two pairs of cantilever radial displacement transducers (CRDT) measured the radial displacements. A fully programmable 6-channel datalogger received the analogue signals from the LVDT's and CRDT's. The analogue/digital conversion was executed by a 13-bit successive approximation technique.

Experimental Program

All discontinuities were submitted to cycles of loading and unloading prior to starting the hydro-mechanical tests. These pre-loading cycles were performed to properly seat the discontinuity halves. Four test cycles were performed, with confining pressures of 2, 3, 5, and 5 MPa, respectively. A low confining pressure and a low hydraulic gradient were applied after the pre-loading cycles to bleed air from the water pressure system and the discontinuity.

The confining pressure and the differential water pressure were controlled during the hydro-mechanical tests. The diametrical deformation normal to the discontinuity and the flow rate were also measured. The effective normal stress acting on the discontinuity depends on the water pressure and confining stress. However, the water pressure is not constant across the discontinuity, thus the effective normal stress is calculated by considering the average of the upstream and downstream water pressure. To keep the non-uniform stress to an acceptable level the minimum effective normal stress was never less than the differential water pressure multiplied by a factor of two.

Generally, four test cycles were applied to the discontinuity samples. Each cycle was performed with a constant differential water pressure and varying effective pressure. The four cycles had different downstream water pressures of about 0.17, 0.15, 0.13 and 0.10 MPa, respectively, and a constant upstream water pressure of 0.2 MPa. The upper limit of the downstream water pressure was determined by the limitations of the equipment. Lower downstream water pressures would have caused the onset of turbulent flow, which was not considered in this study. The confining pressure was set to a relatively low value of 0.1 MPa to 0.5 MPa at the start of each cycle. This was considered the reference point of the specific cycle. Then the confining pressure was increased such that the effective normal stress would reach the desired value when the water pressure was set to the predefined magnitudes. Each cycle consisted of five steps of increasing effective pressure: 0.5, 1, 2, 3, and 5 MPa. In some cases, especially with low differential water pressures, the cycle was ended before reaching the highest effective pressure due to very low flow rates.

Each step of a particular cycle would be maintained until the diametrical deformation and flow rate stabilised.

Cubic Law Validation

The cubic law model describes the fluid flow through a single discontinuity with the assumptions of laminar flow, and parallel and planar discontinuity surfaces. Some authors reported that the cubic law may also be applied to rough discontinuity surfaces with areas of contact between the opposing walls [12, 13, 14].

The validity of the cubic law within the applied normal stress range is verified for the natural and induced tension discontinuities. The methodology applied by Elliot et al. [13], and Lamas [3] was used for this study for each test cycle.

The key point in the analysis is the introduction of the hydro-mechanical coupling parameter, f_{HM}, which correlates the mechanical aperture to the hydraulic aperture. The hydraulic aperture, e_h, is calculated by assuming the validity of the cubic law:

$$Q = \frac{Wg}{12\nu}(e_h)^3 J = C_o (e_h)^3 J$$

The kinetic viscosity, ν, of the water was considered equal to 10^{-6} m²/s at a temperature of about 20°C. The discontinuity width, W, equalled 54 mm. The value of C_o then equals 4.41×10^3 s^{-1}.

To obtain the hydro-mechanical coupling parameter f_{HM}, the calculated hydraulic apertures and corresponding measured relative discontinuity displacements can be plotted in a graph. A linear regression analysis results in the determination of

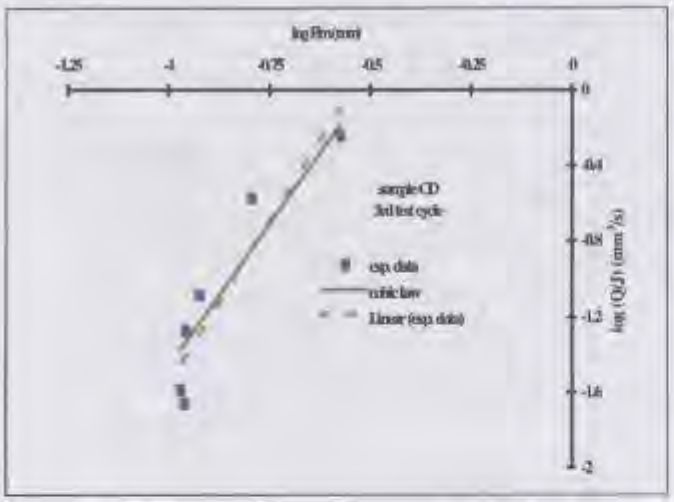

Figure 4. Cubic Law Validation

the best adjusting straight line. The slope of this line equals the value of the coupling parameter. The obtained value of the coupling parameter for each sample is presented in Table 5.

The coupling parameter for each sample is very low, indicating reduced flow rates compared with what would be expected with a laminar flow through parallel and planar discontinuities. Crushing of wall material during loading could have caused obstruction of the flow path. Roughness and degree of interconnection between regions with relative large apertures control the tortuous flow path of the water. The maximum closure, δ_n^{max} of a discontinuity, relative to the specific initial normal stress, can be obtained by assuming that the maximum discontinuity displacement has been reached when the hydraulic aperture equals zero. The regression line has to be extrapolated to

Sample	Test Cycle	f_{HM}	$\log(C_o f_{HM}^3)$ (s^{-1})	K_1 (s^{-1})	K_2
MA	1	0.066	1.106	1.111	3.041
	2	0.039	0.418	0.418	3.012
	3	0.027	-0.061	-0.064	3.010
	4	0.032	0.144	0.141	3.015
MB	1	0.106	1.721	1.732	3.023
	2	0.063	1.041	1.046	3.027
	3	0.085	1.438	1.446	3.030
MC	1	0.051	0.757	0.753	3.041
	2	0.059	0.953	0.953	3.022
	3	0.094	1.559	1.568	3.045
	4	0.098	1.617	1.627	3.039
ME	1	0.101	1.663	1.710	3.095
	2	0.110	1.769	1.789	3.047
	3	0.155	2.212	2.280	3.087
	4	0.209	2.603	2.717	3.153
CA	global	0.105	1.710	2.011	3.332
CC	1	0.089	1.496	1.886	3.481
	2	0.062	1.030	1.124	3.146
	3	0.084	1.418	1.869	3.506
	4	0.063	1.037	1.181	3.204
CD	1	0.098	1.612	1.835	3.321
	2	0.097	1.609	1.867	3.347
	3	0.092	1.529	1.795	3.345
	4	0.100	1.644	1.971	3.384
CE	1	0.033	0.193	0.445	3.735
	2	0.029	0.032	0.140	3.233

Table 5. Hydro-mechanical parameters and cubic law validation

the point of intersection with the horizontal axis, this intersection point corresponds with the maximum closure. Then, the mechanical aperture of the discontinuity can be calculated as:

$$E_m = \delta_n^{max} - \delta_n$$

The obtained experimental data is plotted in a double log plot of Q/J vs E_m (Figure 4).

A linear regression analysis provides a best fitting straight line that can be represented by the following function:

$$\log\left(\frac{Q}{J}\right) = K_1 + K_2 \log(E_m)$$

Assuming that the cubic law is valid, K_1 equals $C_o f_{HM}^3$ and K_2 equals 3.

Comparison of the constants K_1 and K_2 with the corresponding constants of the theoretical line allows a verification of the validity of the cubic law. The values of the theoretical interception point of the vertical axis and experimentally determined constants are given in Table 5.

The constants of the experimental line of the Miranda samples are in close agreement with those of the theory. This implies that reasonable flow predictions can be made with the cubic law for these particular samples and applied test conditions using the hydro-mechanical coupling parameter. The predicted flow rates of the samples CC, CD, and CE do not adjust well to the measured ones. Generally, power values higher than three are found. The flow through the discontinuity samples of Castelo do Bode reveal a deviation from the cubic law, in particular at the range of small apertures. A rapid decrease in the normalised flow takes place at a certain critical aperture that cannot be explained by the cubic law (Figure 4).

Transmissivity as function of stress

The cubic law does not seem to be valid for good fitting discontinuities with rough discontinuity walls and areas of contact between the opposing walls. Therefore, the discontinuity transmissivity T was compared with the effective stress. The transmissivity is defined as:

$$T = \frac{Q}{JW}$$

where,
Q = flowrate [mm³/s]
J = hydraulic gradient [-]
W = discontinuity width [mm]

The graphs in Figure 5 present the typical difference between an induced tension discontinuity and a natural discontinuity.

In particular, the more rapid decrease in transmissivity for the induced tension discontinuities. The samples of Miranda do not show a strong non-linear decrease in transmissivity with an asymptotic value for higher effective stresses. The induced ten-

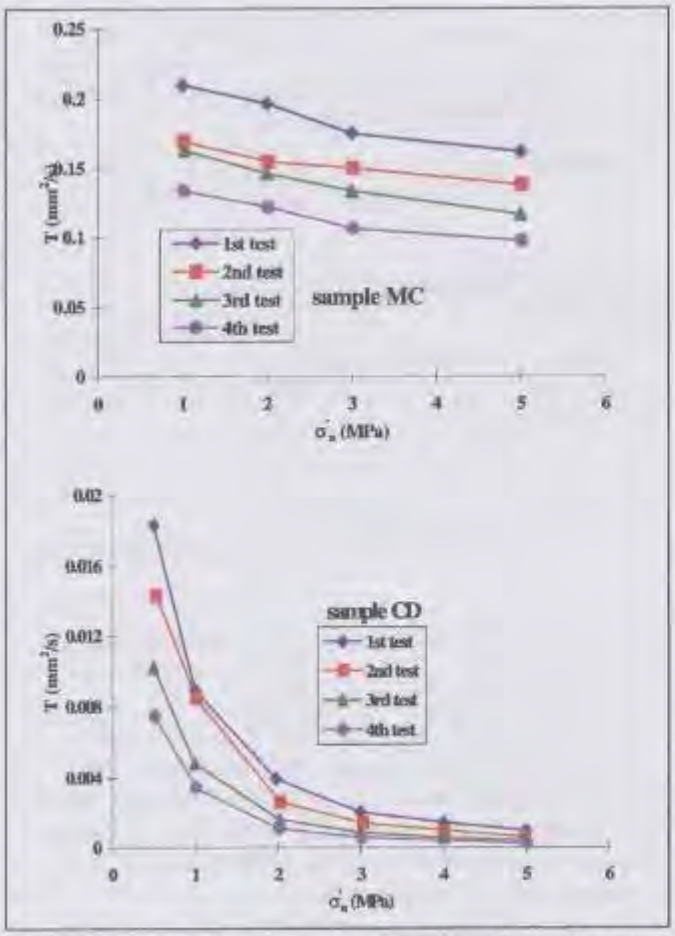

Figure 5. Transmissivity versus Effective Stress for samples CD and MC

sion discontinuities clearly show this phenomenon. This difference is probably related to the roughness and tight fitting of the artificial discontinuities.

A power law is assumed between the transmissivity and applied effective stress for each loading cycle in order to fit the obtained experimental data [15, 16]:

$$T = T_0 \left[\frac{\sigma'_n}{[Pa]} \right]^{-\upsilon}$$

Where T_0 is the transmissivity at an effective normal stress of 1 MPa and where unit [Pa] is introduced for the units to be equal on both sides of the equal sign. By plotting logT vs logσ'_n and using a linear regression analysis, the power term υ is determined as the slope of the regression line. The obtained values for each test cycle and discontinuity sample are presented in Table 6.

High correlation coefficients are found between 0.958 and 1 for the linear relation between the logarithm of transmissivity and logarithm of applied effective normal stress. The intercept T_0 generally decreased with the number of applied test cycles, except for the samples MB and ME. All the Miranda samples have a higher transmissivity and lower values of υ compared with the natural and induced tension discontinuities of the Castelo do Bode samples. The combination of the lower transmissivity and higher value of υ for the Castelo do Bode sam-

Sample	Test Cycle	T_0 (mm²/s)	υ
MA	1	0.124	0.294
	2	0.110	0.153
	3	0.071	0.134
	4	0.058	0.098
MB	1	0.044	0.290
	2	0.081	0.158
	3	0.066	0.152
MC	1	0.214	0.169
	2	0.170	0.126
	3	0.166	0.212
	4	0.136	0.205
ME	1	0.045	0.420
	2	0.075	0.246
	3	0.025	0.704
	4	0.068	0.629
CA	1	0.0011	1.385
	2	0.0008	2.313
CC	1	0.0023	1.785
	2	0.0016	1.528
	3	0.0015	1.765
	4	0.0011	1.543

Table 6. Parameter values relating transmissivity to effective stress

ples seems to be related to the geometrical properties and degree of fitting of these discontinuities. The natural discontinuity CA is undulated and the induced tension discontinuities have surfaces with large and sharp asperities. The water flows through small interconnected channels with increasing stress, these channels cause the path to become tortuous. These discontinuities also have a tight fitting, causing the discontinuity to close easily with increasing normal stress as was experienced during the tests.

Conclusions

The roughness characterisations lead to several conclusions:

- A finite element technique allows a relatively easy calculation of the roughness indexes and the statistical parameters for irregularly spaced data points.
- The variance of the asperity heights can be a good indicator of the surface roughness and no specific distribution of the asperity heights could be distinguished.
- Good correlation between the experimentally determined JRC and the calculated roughness indexes was found for the used scanning procedure.

From the statistical analysis of the aperture distribution a number of conclusions can be drawn:

- A significant difference between the harmonic and arithmetic mean was observed, The harmonic mean is considered more appropriate.
- All aperture distributions are right tailed and have a high concentration around the mean.
- It appears that the natural discontinuities have small-scale channels with a preferred direction.

The following can be concluded for the hydro-mechanical characterisation:

- Low values for the hydro-mechanical coupling parameter were found for all the samples, implying that smaller flow rates were obtained than what would be expected with those predicted by the cubic law.
- Generally, the flow rates predicted with the cubic law using the hydro-mechanical coupling parameter are in agreement with the experimentally obtained flow rates of the Miranda samples. For the induced tension discontinuities of Castelo do Bode with rougher surfaces and good fitting, a more rapid decrease of the flow rate with decreasing aperture is obtained.
- The induced tension discontinuities have, compared with the natural discontinuities of Miranda, a lower transmissivity with a stronger non-linear decrease of the transmissivity that tends asymptotically to a low value. This difference is probably related to the geometrical properties and degree of fitting.
- The power law, which relates the transmissivity to the applied effective stress, adjusts well to the experimental data.

References

1. Vicente, Silvestre M.V. 1996. "Geometrical and Hydro-mechanical Characterization of Discontinuities," MS Thesis, Delft University of Technology, Delft.

2. Gentier, S. 1986. "Morphology and hydro-mechanical behaviour of a natural fracture in granite under normal stress" (in French), Ph.D. Thesis, University of Orléans, Orléans.

3. Lamas, L.N. 1993. "Contributions to understanding the hydromechanical behaviour of pressure tunnels," Ph.D. Thesis, Imperial College, London.

4. Muralha, J. 1995. "Mechanical behaviour of discontinuities of rock masses" (in Portuguese), Ph.D. Thesis, Technical University of Lisbon.

5. Zienkiewicz, O.C. 1977. *The Finite Element Method*, 3rd edition. McGraw-Hill Book Company (UK) Limited, London.

6. Louis, C. 1968. "A Study of Groundwater Flow in Jointed Rock and its Influence on the Stability of Rock Masses (in French), Ph.D. Thesis, University of Karlsruhe, Karlsruhe.

7. Myers, N.O. 1962. "Characterization of Surface Roughness." *Wear*. 5, 182-189.

8. Barton N. and V. Choubey. 1977. "The shear strength of rock joints in theory and practice," *Rock Mech.*, 10(1-2) 1-54.

9. Tse, R., and D.M. Cruden. 1979. "Estimating Joint Roughness Coefficients, *Int. J. Rock Mech. Min. Sci. & Geomech. Abstr.* 16, 303-307.

10. Yu, X., and B. Vayssade. 1991. "Joint profiles and their roughness parameters," *Int. J. Rock Mech. Min. Sci. & Geomech. Abstr.* 28 (4) 333-336.

11. Hakami, E., Einstein, H.H., Gentier, S. and M. Iwano 1995. "Characterisation of fracture apertures," *Proc. 8th Congress Int. Soc. Rock Mechanics*, 2, 751-754, Tokyo.

12. Witherspoon, P.A., Wang, J.S.Y., Iwai, K., and J.E. Gale. 1980. "Validity of cubic law for fluid flow in a deformable rock fracture," *Water Resources Res.*

—*continued on page 23*

Figure 16. Uniaxial compression test of marble model pillars under lateral confinement given by rubble to simulate filling

value, as well as environmental advantages for not creating huge block piles at the surface.

The results obtained upon these experiments indicate a clear increase of compressive strengths in the model pillars, which depends on the correct lay-out of the support system that is chosen in each case, as well as their mechanical resistance.

That increment of strength can be observed by the corresponding Mohr circles (Figure 17), indicating several orders of magnitude of increment, with respect to the shear strength of the unsupported pillars.

Conclusions

A series of laboratory and numerical studies were developed in order to create a data base for the design of a new underground exploitation unit of marble in Portugal. Special tests were performed to supply detailed information on the behaviour of structures that will be excavated, and their critical stress and strain values were determined to obtain guidelines for that design, particularly on the safety aspects. Furthermore, simulation of applied support systems provided insight on their applicability and efficiency.

Acknowledgements

The author wishes to acknowledge the cooperation of Professors Yu Xianbin and Matilde Silva in the research work that was developed.

The IGM and IAPMEI offices are sincerely thanked for the sponsorship provided for the investigation that was reported in the article.

References

Agapito, J.F.T. 1986. "Pillar Stability In Large Underground Openings: Applications From A Case Study In Competent, Jointed Rock." Quarterly 81(3). Colorado School Of Mines. Colorado.

Brady, B.H.G. and E.T. Brown. 1985. Rock Mechanics For Underground Mining. George Allen & Unwin. London.

Dinis Da Gama, C. and Yu Xianbin. 1999. Geomechanical Investigations In a Multiple Room and Pillar Mine." *Proceedings 9th International Congress On Rock Mechanics*, Paris. A. Balkema, Rotterdam. 1, 259-263.

Franklin, J.A. and M. Palassi. 1993. "Maximum Span and Stand-Up-Time Of Underground Excavations," *Proc. Innov. Mine Design For The 21 St Century*, Bawden & Archibald (Eds), Balkema.

Hoek, E. and E.T. Brown. 1980. "Underground Excavations In Rock." The Institution of Mining and Metallurgy. London.

Hoek, E; Kaiser, P. K. and W. F. Bawden. 1998. "Support of Underground Excavations In Hard Rock." A.A. Balkema. Rotterdam. Brookfield.

Hutchinson, D. J. and Diederichs. 1996. "Cablebolting In Underground Mines." Bitech Pbls. Richmond.

Jaeger, J. C. 1974. "Elasticity, Fracture And Flow." Science Paperbacks, London.

Obert, L. and W. I. Duvall. 1967. "Rock Mechanics and the Design Of Structures In Rock." John Wiley & Sons. New York.

Pakalnis, R. and S. Vongpaisal. 1993. "Mine Design—An Empirical Approach." *Proc. Innov. Mine Design for the 21st Century*, Bawden & Archibald (Eds). Balkema.

Parker, J. 1973. "Practical Rock Mechanics For Miners." *Engineering And Mining Journal*, June-December 1973, January-February 1974.

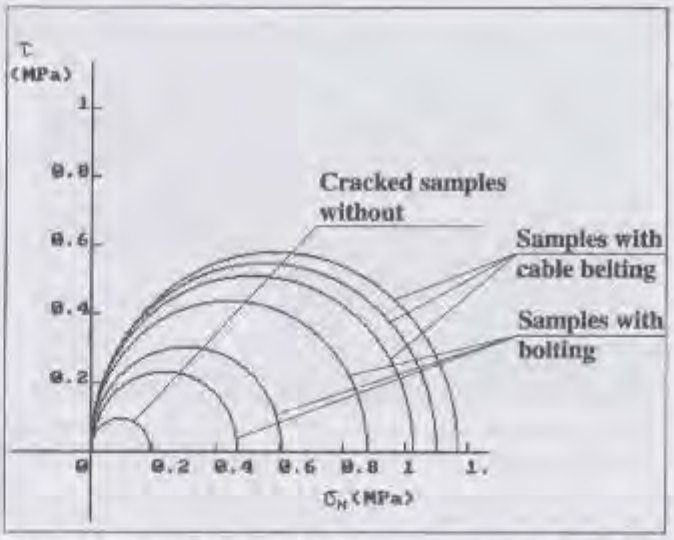

Figure 17. Mohr circles of failures in marble pillar models with and without artificial support systems

---

Laboratory Study, —continued from page 15

16 (6), 1016-1024.

13. Elliot, G.M., Brown, E.T., Boodt, P.I., and J.A. Hudson. 1985. "Hydromechanical behaviour of joints in the Carnmenellis granite, S.W. England," *Proc. Int. Symp. On Fundamentals of Rock Joints*, Björkliden.

14. Zhao, J. 1987. "Experimental Studies of the Hydro-Thermal-Mechanical Behaviour of Rock Joints in Granite," Ph.D. Thesis, Imperial College, London.

15. Raven, K.G., and J.E. Gale. 1985. "Water Flow in a Natural Rock Fracture as a Function of Stress and Sample Size," *Int. J. Rock Mech. Min. Sci. & Geomech. Abstr.*, 22 (4), 251-261.

16. Iwano, M. 1995. "Hydromechanical Characteristics of a Single Rock Joint," Ph.D. Thesis, MIT, Massachusetts.

Société Internationale de Mécanique des Roches
INTERNATIONAL SOCIETY FOR ROCK MECHANICS
Internationale Gesellschaft für Felsmechanik
NEWS JOURNAL

Volume 7, Number 2 — June 2002

Senior Editor
Prof. Marc Panet, President ISRM
GS Ingénierie
10, Av. Newton
92350 Le Plessy Robinson
France
Telephone: 33.1.460.12410
Fax: 33.1.463.28291
E-mail: marc.panet@fcinternational.com

Contributing Editor
Send news of meetings and publications to:
N. F. Grossmann
ISRM Secretariat, c/o LNEC
101 Avenida do Brasil
P–1799 Lisboa Codex, Portugal
Telephone: 351.1.848.2131
Fax: 351.1.847.8187
Telex: 16760 LNEC

Managing Editor
Send articles, advertising and other material to:
Jennifer Bartholomew
2112 Drew Avenue South
Minneapolis, MN 55416 USA
Telephone: 612.926.8196
Fax: 612.926.6416
E-Mail: jkbart@usinternet.com

ISRM Secretariat
José Delgado Rodrigues, Secretary-General
E-mail: delgado@lnec.pt
Maria de Lourdes Eusébio, Executive Secretary
E-mail: isrm@lnec.pt
The ISRM Secretariat, LNEC
101 Avenida do Brasil
P–1799 Lisbon Codex, Portugal
Telephone: 351.21.844.3419
Fax: 351.21.844.3021

ISRM Homepage
http://www.lnec.pt/ISRM/

Back issues ($8) are available from the Secretariat.

Rocha Medal

A Bronze Medal and cash prize has been awarded annually since 1982 by the ISRM to honour the memory of Past President Manuel Rocha and to recognize outstanding young researchers in the field of Rock Mechanics.

The award shall be for an outstanding doctoral thesis in rock mechanics or rock engineering. The thesis must have qualified the candidate for a doctorate or the equivalent. To be considered for the award, a candidate must be nominated within two years of the date of the official doctoral degree certificate. The nomination should be submitted to the appropriate ISRM Regional Vice-President by registered letter, and may be presented by the nominee, the nominee's National Group or some other person or organization acquainted with the nominee's work. The nomination should include the following supporting information:

- *A one page curriculum vitae*, including the name, nationality, place and date of birth of the nominee; also position, address, telephone and fax numbers;
- *A thesis summary* in one of the official languages of the Society, preferably English, of about 5,000 words, detailed enough to convey the full impact of the thesis, and accompanied by selected tables and figures, with headings and captions also in English;
- *One copy of the complete thesis* and *one copy of the doctoral degree certificate;*
- *A letter of copyright release*, allowing the ISRM to make copies for review & selection purposes only.

Nominations for the 2003 Rocha Medal must be received by 31 December 2002.

Supplementary details of the selection procedure, conferring of the award, etc., are provided in ISRM By-Law No. 7, found on pages 30–31 of the ISRM Directory for 2000. National Groups and Corresponding Members will be officially reminded by the Secretariat as the deadline approaches, but are encouraged to consider possible nominees and to recommend names to the appropriate ISRM Regional Vice-President as early as possible.